JAMES | Journal of Advances in Modeling Earth Systems

RESEARCH ARTICLE
10.1029/2019MS002006

Key Points:
- A method is presented to nudge a cloud fraction parameter in a global coupled forecast system to reduce surface net shortwave flux biases.
- Results from a series of 45-day test forecasts are presented demonstrating the efficacy of the approach.
- Further tests are required to determine operational applicability using a suitable near real-time source of surface radiative flux data.

Correspondence to:
J. A. Ridout,
james.ridout@nrlmry.navy.mil

Citation:
Ridout, J. A., Barton, N. P., Janiga, M. A., Reynolds, C. A., May, J. C., Rowley, C., & Bishop, C. H. (2021). Surface Radiative flux Bias reduction through regionally varying cloud fraction parameter nudging in a global coupled forecast system. *Journal of Advances in Modeling Earth Systems*, *13*, e2019MS002006. https://doi.org/10.1029/2019MS002006

Received 24 DEC 2019
Accepted 14 APR 2020
Accepted article online 21 APR 2020

Surface Radiative Flux Bias Reduction Through Regionally Varying Cloud Fraction Parameter Nudging in a Global Coupled Forecast System

James A. Ridout[1], Neil P. Barton[1], Matthew A. Janiga[1], Carolyn A. Reynolds[1], Jackie C. May[2], Clark Rowley[2], and Craig H. Bishop[3]

[1]Marine Meteorology Division, Naval Research Laboratory, Monterey, CA, [2]Ocean Sciences Division, Naval Research Laboratory, Stennis Space Center, MS, [3]School of Earth Sciences and ARC Centre of Excellence for Climate Extremes, The University of Melbourne, VIC, Australia

Abstract A simple parameter nudging procedure is described that systematically reduces near-analysis time errors in the surface net shortwave flux in the Navy ESPC (Earth System Prediction Capability) system, a global coupled forecast system that is the product of a continuing development effort at the U. S. Naval Research Laboratory. The procedure generates geographically varying perturbations to one of the cloud fraction parameters in the atmospheric model component of the system during the data assimilation cycle, resulting in large improvements in near-analysis time surface net shortwave flux biases. After a several week spin-up period, the global RMSE of the succeeding 10-day mean bias computed for lead times of 6–12 hours is reduced by 40 percent. Results from application of the approach in a series of 45-day integrations show that improvements are realized at longer forecast lead times as well. The global RMSE of the surface net shortwave flux averaged over these integrations improves by 37 percent for lead times from 1–5 days, decreasing to 18 percent for lead times from 31–45 days. The corresponding longwave flux errors are slightly degraded, ranging from a 2 percent increase for lead times from 1–5 days to a 0.5 percent increase for lead times from 31–45 days. Global-mean reductions in ground and sea surface temperature errors are obtained through most of the 45-day integration period due to improvements over ocean and polar regions. Potential steps for extension and operational application of the method are discussed.

Plain Language Summary The net radiation budget at the earth's surface is of key importance for weather and climate, and clouds are a primary agent in regulating this budget. This study presents a simple but powerful method to gradually adjust the cloud cover in weather and seasonal forecast models during the process of forecast initiation in a way that brings the model surface radiation budget into better agreement with satellite observations. Improvements to ground and sea surface temperature forecasts are highlighted in addition to reductions in surface radiation budget errors.

1. Introduction

The representation of clouds and their radiative effects has long been recognized as a key challenge for numerical weather and climate models, requiring model fidelity to not only the direct radiative impact of clouds but more broadly the hydrological cycle as it functions to define the occurrence and structure of cloud fields (e.g., Cess et al., 1990). Progress towards these goals has been considerable over the past decades, yet considerable challenges remain (e.g., Calisto et al., 2014; Yin & Porporato, 2017). Advances in process understanding and computational resources have not eliminated the need, for example, for rendering of physical processes through parameterizations comprised typically of a simplified, but physically based algorithm with specified values for certain quantities (parameters). The suitability of given parameter values may vary with conditions; hence values are sometimes specified differently in different forecast ensemble members (e.g., Reynolds et al., 2011) or assigned in a stochastic manner (e.g., Hansen and Penland 2007; Ollinaho et al., 2017) to represent the effects of expected variability. Not uncommonly, optimal parameter values will change with changes in other features of the physics suite utilized in the model or changes in the model resolution, and a considerable amount of computing time can be needed to adjust parameters in such cases.

Strategies for parameter adjustment (or "tuning") vary (e.g., Schmidt et al., 2017). Several studies have reported on ensemble-based Kalman filters used for quantitative parameter estimation (e.g., Aksoy et al., 2006; Anderson, 2001; Hacker & Snyder, 2005; Li et al., 2018). In these studies, the data assimilation update cycle includes estimation of both the initial state and parameter values. In the spatial average method described in Aksoy et al. (2006) for a limited-area weather prediction model, and refined by Liu et al. (2014) for a coupled global climate model, the parameter update varies spatially, but one spatially-averaged parameter is fed into the next update cycle. Wu et al. (2012) use an intermediate complexity coupled model to investigate a method which allows for a geographic-dependent parameter optimization, and find the geographic dependent technique superior to the single-value parameter estimation technique for both climate estimates and predictions. Recently, Zhao et al. (2019) found that ensemble-based Kalman Filter parameter optimization in the Zebiak-Cane model (Zebiak & Cane, 1987) improves El Nino Southern Oscillation prediction skill. Other techniques for parameter estimation include Markov chain Monte Carlo algorithms (e.g., Posselt & Bishop, 2012), and gradient descent and genetic algorithms (e.g., Sumata et al., 2013).

The overview article by Hourdin et al. (2017) notes that cloud fraction (along with cloud microphysics and convection) is one of the most common parameterizations adjusted during the tuning of climate models. In the current study, a single parameter in the Xu and Randall (1996a) cloud fraction scheme is adjusted through an iterative nudging procedure in a manner that attempts to account for geographically varying cloud biases. In contrast to most of the previous parameter estimation techniques reported on, this method uses a variational data assimilation scheme rather than an ensemble-based Kalman Filter. The method is described in section 2 and preliminary test results with the Navy Earth System Prediction Capability (ESPC) system are presented in section 3. Section 4 concludes with a discussion and summary.

2. Iterative Cloud Fraction Parameter Adjustment

The cloud fraction parameter adjustment procedure developed in this study represents an effort to reduce surface radiative flux biases in the Navy ESPC system, a global coupled system developed by the U.S. Naval Research Laboratory. This system is comprised of the Navy Global Environmental Model (NAVGEM) (Hogan et al., 2014) coupled to the Global Ocean Forecast System (GOFS) (Metzger et al., 2014), which includes both the Hybrid Coordinate Ocean Model (HYCOM) (Bleck, 2002) and the Los Alamos Community Ice Code (CICE), version 4.1 (Hunke & Lipscomb, 2010). Radiative fluxes and associated heating are computed using the Rapid Radiative Transfer Model for general circulation models (RRTMG) scheme (Iacono et al., 2008). Cloud water and ice condensate in NAVGEM are parameterized with an extension of the treatment of Zhao and Carr 1997. Cloud fractions are computed using the Xu-Randall scheme (1996a) for stratiform clouds and a modified version of the treatment of Slingo (1987) for convective clouds (see Appendix). The Xu-Randall scheme is the focus of the parameter adjustment effort described here. The reader is referred to Janiga et al. (2018) for further summary of the physics in the NAVGEM implementation in the coupled system.

2.1. Xu-Randall Cloud Fraction Parameterization in NAVGEM

The Xu-Randall cloud fraction scheme parameterizes cloud fraction based on relative humidity RH, saturation specific humidity q_s and cloud condensate mixing ratio q_c (Xu & Randall, 1996a). The scheme provides an estimate of the stratiform cloud fraction cf_{strat} using the relation:

$$cf_{strat} = RH^{k_1}\left[1 - \exp\left(-\frac{k_2\, q_c}{[(1-RH)\, q_s]^{k_3}}\right)\right], \tag{1}$$

where k_1, k_2, and k_3 are constant parameters. For q_c NAVGEM uses an estimate of the cloud condensate mixing ratio associated with stratiform clouds obtained simply from the total prognostic condensate moist mixing ratio q_t. The partitioning is carried out using the parameterized convective cloud fraction (cf_{conv}, see Appendix) together with diagnostic estimates of in-cloud cloud water (cf. Ridout et al., 1994) adopted from the Navy Operational Global Atmospheric Prediction System (NOGAPS) (Hogan & Rosmond, 1991) radiation scheme (Harshvardhan et al., 1987). For details, see Appendix. The constant parameters k_1, k_2, and k_3 are currently set to 0.50, 45.0 and 0.64, respectively, in the Navy ESPC system, the result of an effort to improve global means of cloud cover and top of the atmosphere radiative fluxes. These settings differ from

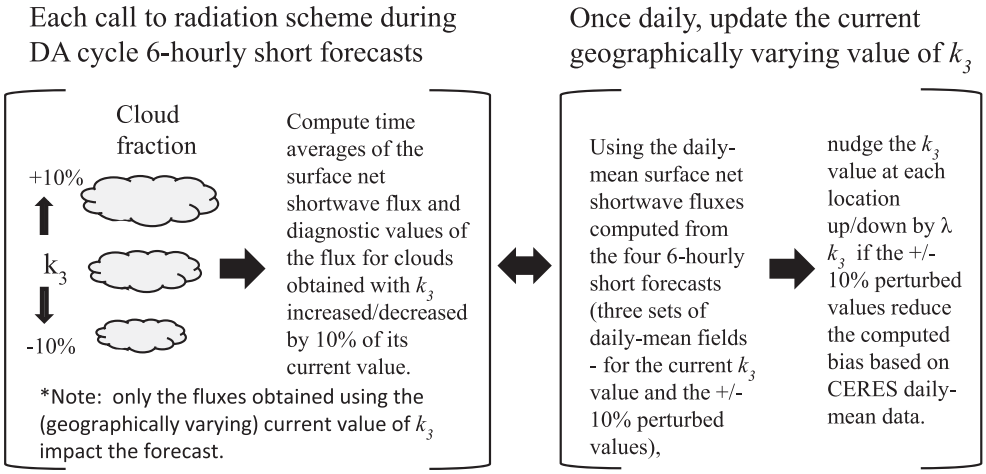

Figure 1. Schematic view of the parameter nudging procedure during the DA cycle.

those in the published scheme, which assigns values of 0.25, 100.0, and 0.49, respectively, based on an explicit two-dimensional simulation of clouds that occurred during GATE in the tropical Atlantic (Xu & Randall, 1996b). Notably, the published values have been used with some success in the National Centers for Environmental Prediction (NCEP) Global Forecast System (GFS) (e.g., Ye & Chen, 2013). Nonetheless, differences with respect to the published values are not unreasonable given the expectation that optimal values from a global perspective might differ from those obtained from the published regional GATE simulation.

2.2. Parameter Nudging

The parameter nudging procedure developed in this study applies a simple iterative adjustment to parameter k_3 in (1), to which we have found the parameterized cloud fractions to be particularly sensitive. This procedure slightly adjusts the value of k_3 during the data assimilation (DA) cycle by a regionally varying amount once per forecast day in the direction that reduces the local daily mean surface net shortwave flux bias with respect to satellite retrieved fluxes. To accomplish this step, when the parameter adjustment scheme is activated, 3-hourly mean radiative flux fields are saved from the 6-hourly short forecasts in the DA cycle used to provide first guess fields. The saved radiative flux data include values obtained diagnostically using values of the k_3 parameter increased/decreased by ten percent of its value for the given day at each hourly call of the radiation scheme. Thus three sets of time-averaged radiative flux data are saved from each of the DA cycle short forecasts. Daily mean surface shortwave fluxes are constructed from these 3-hourly mean fields using the output for lead times from 6–12 hours in an effort to help minimize impacts of model spin up. Once per day these daily mean fluxes are compared on a 1 x 1 degree latitude/longitude grid against a satellite-based retrieval, currently the NASA Clouds and the Earth's Radiant Energy System (CERES) daily mean surface shortwave product (Doelling et al., 2013). If the computed model bias is less for the results obtained with the increased/decreased parameter value, the parameter is simply adjusted upward/downward by a tunable factor λ (currently 0.02). In other words, any parameter adjustments made for a given day are simply equal to (plus/minus) $\lambda\, k_3$. The procedure is illustrated schematically in Figure 1. Although the resultant parameter adjustments for any given day are small, the perturbed parameter values can over time become significant. Limits on the value of k_3 would thus be required for operational implementation. Our initial DA cycle testing used no such limit until after the period from which the long forecasts discussed in the following section were initialized. Lower and upper bounds of 0.1 and 1.0 on k_3 were subsequently applied, but further testing is needed to determine the sensitivity to these limits.

The cost of implementing the procedure within the DA cycle is fairly minimal. The total cost of the DA cycle in the coupled system is dominated by the short forecasts. Although the extra calls to the radiation scheme increase the computational cost of NAVGEM in the short forecasts by approximately 10%, the cost of the forecasts is still dominated by HYCOM. Because of the disparate timing of the model components, in fact,

Table 1
Navy ESPC test runs

CTL – Control run PP – Perturbed Parameter run
Spin-up from July 31, 12Z Forecasts from Sept. 1, 6, 11, 16, 21, 26, Oct. 1, 6, 11, 16, 21, 26, 31, and Nov. 5, 10 2013 (12Z)

typically NAVGEM must wait for HYCOM to finish before the coupling exchanges between the models can occur. For the long forecasts, at least in the simple application of the scheme used in this study, there is essentially no additional cost, since the system simply uses the map of k_3 values valid at the forecast initiation time computed during the DA cycle.

Significant regional variations in the k_3 parameter value develop over the course of one to two weeks with the simple procedure outlined here, which by design targets a gradual but systematic reduction in regional cloud cover biases while avoiding overly noisy parameter field variations that might arise through larger instantaneous adjustments or stronger minimization constraint approaches. The scheme thus attempts to address the effects of regionally varying model biases using what is clearly a heuristic method, generating

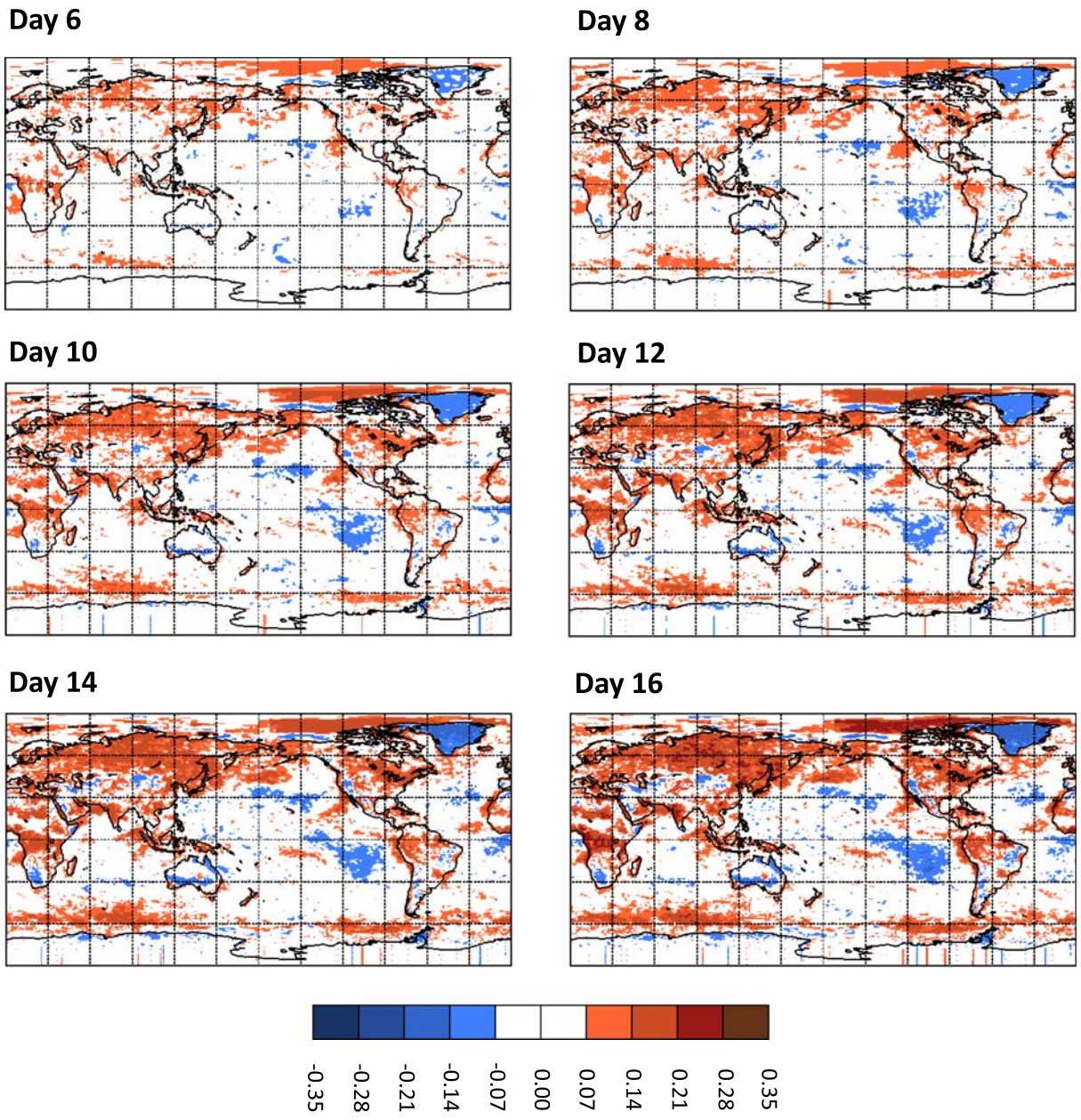

Figure 2. Evolution of perturbations to the *k3* parameter in the Xu-Randall cloud fraction scheme during the first 16 days of the PP DA cycle run with the Navy ESPC system.

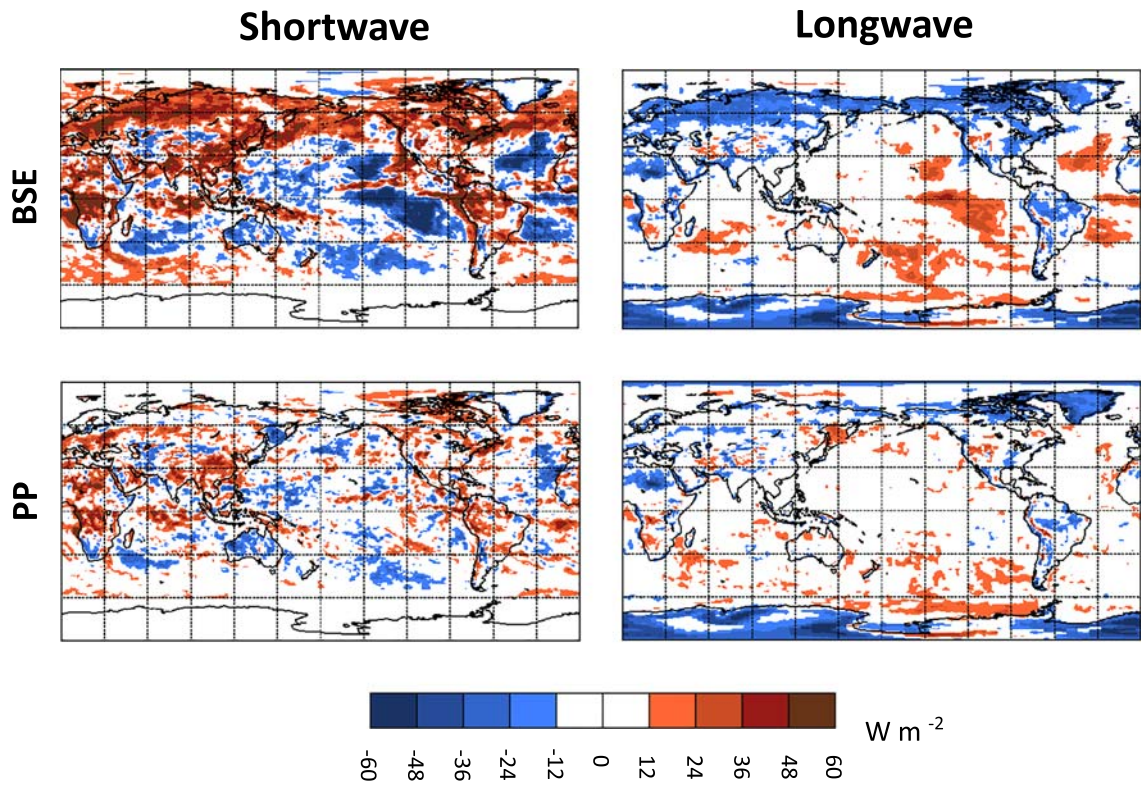

Figure 3. Mean tau 6–12 hour bias (W m^{-2}) in the net downward surface shortwave and longwave fluxes for the last ten days of August 2013 for the CTL and PP runs.

cloud fraction parameter perturbations as a fix for an assortment of uncertain model deficiencies. While the biases in the Navy ESPC system are not yet known as well as for some more established forecast systems, experience with NAVGEM has pointed for example to difficulties associated with the boundary layer physics in representing low cloud cover in some of the tropical/subtropical ocean regions, including west coastal marine stratocumulus. Because the parameter adjustments in effect attempt to moderate the impacts of various such deficiencies, it is emphasized that the generated parameter perturbations do not necessarily reflect negatively on the Xu-Randall parameterization itself. From this perspective, we note that similar considerations may be relevant for parameter tuning efforts more generally. However, the present work, in allowing for geographically varying parameter values, may be more susceptible to anomalous situations. For example, if the model under predicts the amount of cloud condensate in a given region, the scheme would be expected to compensate by adjusting k_3 upwards to increase cloud cover. Over compensation in terms of the impact on cloud cover may in fact occur because in such cases the deficiency in condensate may render the clouds less bright than they should be. Given the uncertainties surrounding such impacts, testing is required to weigh the implications for practical implementation. Towards this end the efficacy of the scheme with respect to its impact on 45-day forecasts is examined in section 3.

3. Initial Application of the Scheme for 45-Day Forecasts

For the tests of the parameter adjustment scheme presented here, the NAVY ESPC system was run in a configuration with NAVGEM horizontal resolution at T359 (~37 km at the equator) and 60 vertical levels, and HYCOM and CICE with a 1/12 degree (~9 km) grid, which allows for the resolution of ocean mesoscale eddies. Two sets of DA cycle runs were carried out starting from initial conditions for 12Z on 31 July 2013. The first was a Control run (CTL**)** with the unperturbed constant value (0.64) for the Xu-Randall k_3 parameter; the second was a "Perturbed Parameter" (PP) run with adjustments to k_3 following the procedure outlined in section 2 above (see Table 1). The time-averaged surface radiative flux data from the 6-hourly short forecasts of the DA cycle were saved from both the CTL and PP runs. In addition, the series of daily values of

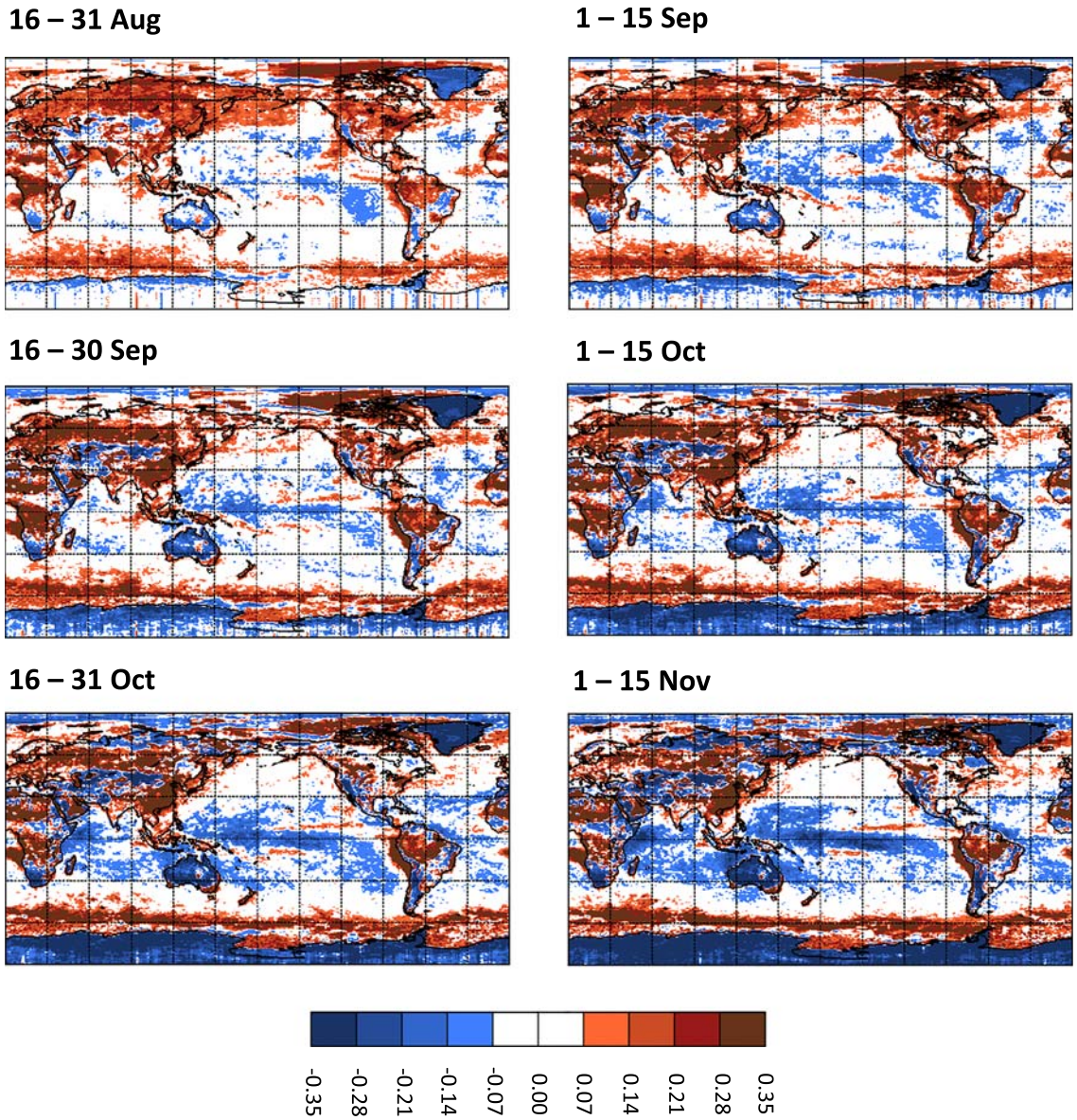

Figure 4. Perturbations to the k_3 parameter in the Xu-Randall cloud fraction scheme computed in the PP run DA cycle averaged over approximately two-week periods extending into November 2013.

the k_3 parameter on a global 1 x 1 degree grid were saved from the PP run. The month of August was taken as a spin-up period for subsequent series of 45-day model integrations carried out to investigate the impact of the k_3 parameter perturbations on extended range forecasts. For both the CTL and PP runs, a total of 15 45-day forecasts, beginning at 12 Z on 1 Sept., 2013 and spaced five days apart, were carried out from restart files created in the DA cycles. In this initial baseline study, for the PP series forecasts the parameter perturbations were maintained constant at the values from the DA run values on the date of initiation.

3.1. DA Cycle Spin-Up Period

The evolution of the parameter perturbations (k_3 value – 0.64) during the first half of the August 2013 spin-up period are shown in the plots in Figure 2. Note that positive perturbations to k_3 tend to increase the cloud fraction. The perturbations by design develop relatively slowly, and as seen here begin to stabilize after ten days or so. There are broad regions of positive perturbation values over many continental regions, with more mixed results over the oceans. The negative values over Greenland may be a reflection of too high

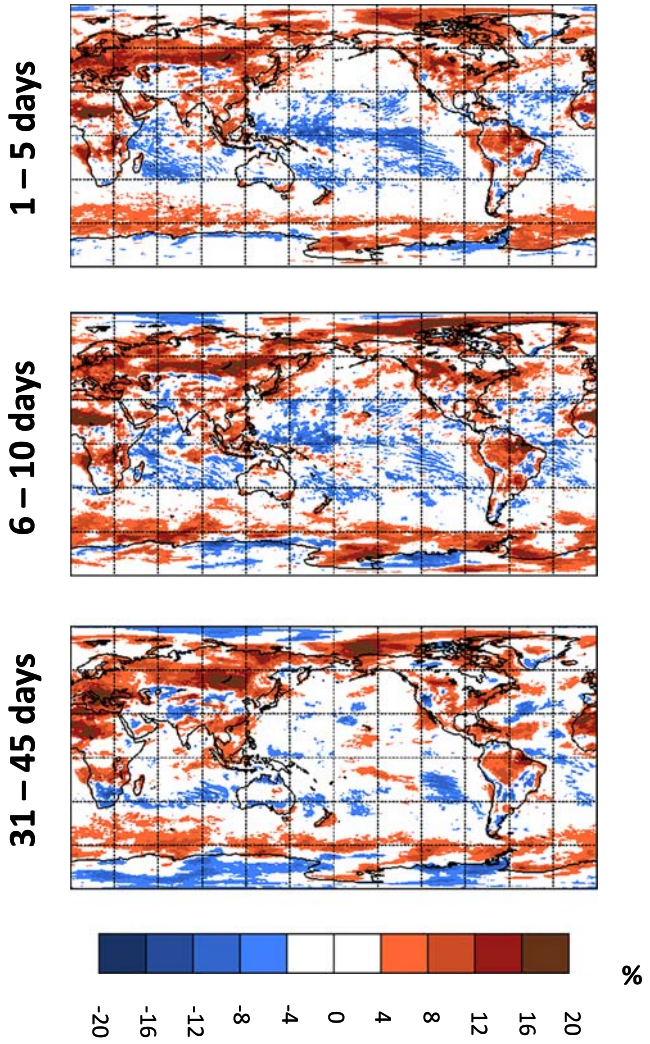

Figure 5. Cloud cover (total coverage in percent) differences between the PP and CTL runs (PP – CTL) for different lead-time averaging intervals.

a surface albedo for the region in NAVGEM, resulting in the scheme adjusting the cloud cover downward to compensate. By the last ten days of August, there is a substantial reduction in the surface net downward radiative flux biases in the short forecasts of the DA cycle. This improvement is evident in Figure 3, which shows the mean bias for both the shortwave and longwave fluxes over the last 10-day period in August as measured with respect to corresponding CERES data for both the CTL and PP DA runs. The model radiative fluxes used to create the plots in Figure 3 are averages of fluxes for lead times of 6–12 hours from the four daily DA cycle short forecasts, following the procedure taken in the implementation of the scheme (section 2). Impacts of the parameter perturbations on surface radiative flux biases for longer lead times are explored in the following subsection. The results plotted in Figure 3 reflect a reduction in the global mean bias in surface net downward shortwave flux in the PP run from 5.1 to 2.4 W m^{-2}, and there is a corresponding 40 percent reduction in the global RMSE of the 10-day mean surface net downward shortwave flux from 24.1 W m^{-2} to 14.6 W m^{-2}. These results illustrate that the treatment is essentially functioning as designed to reduce surface shortwave flux biases near the analysis time. For the longwave fluxes, although the global mean bias of −0.4 W m^{-2} for the CTL run is increased slightly to 1.3 W m^{-2} in the PP run, the global RMSE of the 10-day mean surface net downward longwave flux is reduced from 13.4 W m^{-2} to 10.8 W m^{-2}. Though not as pronounced an improvement as in the case of the surface shortwave fluxes, as reflected in these numbers the scheme is found to improve the representation of surface longwave fluxes near the analysis time over many parts of the globe as well.

3.2. 45-Day Forecast Impacts

The evolution of the k_3 parameter perturbation computed in the PP run DA cycle extending through the period during which the 45-day forecasts were initiated is illustrated in plots in Figure 4, which presents averages over approximately two-week periods. Notably the perturbation map for 16–31 Aug. in Figure 4 is very similar to the Day 16 (16 Aug.) map in Figure 2, supporting the conclusion that the initial spin-up of the parameter perturbations has largely diminished after the first two weeks of the DA cycle. The perturbations do continue to slowly evolve, though some broad similarities persist through the period. In the northern Midlatitudes the positive perturbations that developed in August over land decrease in certain regions, particularly over North America. In contrast, negative perturbations over many oceanic regions in the Tropics and Southern Hemisphere Subtropics continue to grow in magnitude. It should be emphasized that the perturbations are generated in the DA cycle, and reflect biases in the surface shortwave flux at very short lead times. Because model biases typically grow in magnitude with lead time, and also may change over the course of extended range integrations simply because of a changing seasonal bias, the degree to which the generated perturbations can be expected to yield improved surface shortwave fluxes over synoptic timescales and beyond needs to be investigated. As indicated above, the distribution of *k3* parameter perturbations is fixed in time during each of the.

PP series forecasts, set to the distribution obtained in the PP series DA cycle as described in section 2 for the day of the forecast initiation. This approach is adopted here as a baseline test of the method. This treatment may not be optimal, as evident from some of the apparently seasonal changes in the perturbations plotted in Figure 4. Further refinements of the method, including possible application of a generated climatology of perturbations and/or lead-time dependent values will be considered in a future study.

Impacts of the parameter perturbations on cloud cover are shown in Figure 5, which plots the mean difference in total cloud cover between the 15 PP and CTL forecasts over various lead-time intervals assuming maximal cloud overlap. In these plots and in the succeeding radiative flux comparisons, the actual lead

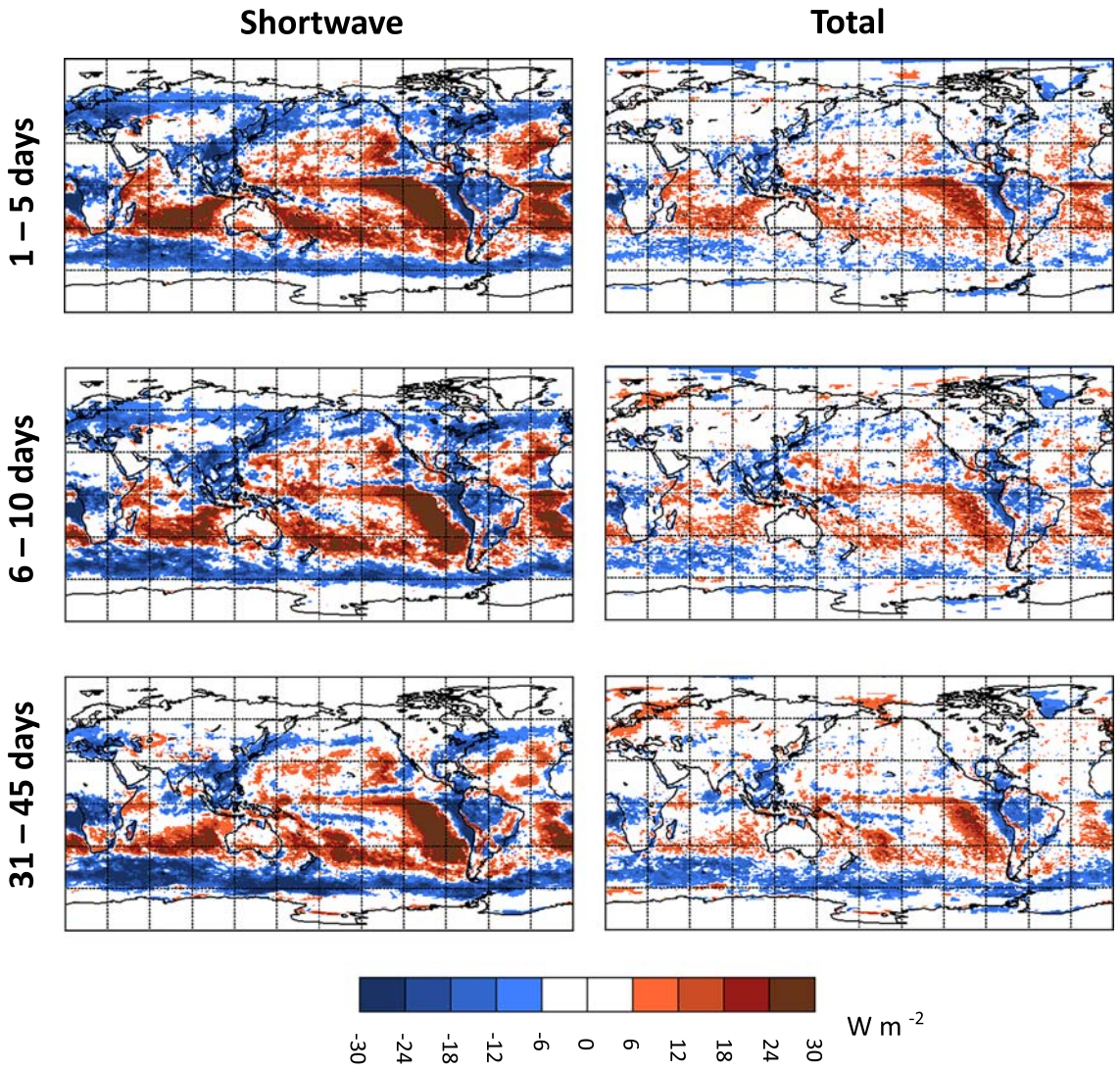

Figure 6. Surface net downward shortwave and total radiative flux differences (W m^{-2}) between the PP and CTL runs (PP – CTL) for different lead-time averaging intervals.

time represented is 12 hours greater than the labeled ranges. The 12-hour offset provides consistency with our utilization of daily mean CERES radiative flux data for radiative flux bias comparisons and is a consequence of the current need to initiate Navy ESPC system runs from 12Z on a given day. In Figure 5 there are considerable similarities in the cloud cover differences for the various lead-time intervals, with enhanced cloud cover over many continental regions and decreased cloud cover over many oceanic portions of the Tropics and Subtropics. Extratropical oceanic regions tend to show an increase in cloud cover in the PP runs, particularly in the Southern Ocean. The cloud cover differences generally show a broad consistency with prevalent patterns in the k_3 parameter perturbation plots in Figure 4. There is a significant decrease, however, in the negative cloud cover changes over the equatorial western Pacific with lead time. This decrease appears to reflect an increase in convective cloud cover in the PP run with respect to the CTL run in the region as the runs progress. The Navy ESPC system does not currently output separately the stratiform and convective cloud cover; however there are increases in convective rainfall differences with lead time (not shown) that would tend to explain the observed trend.

The surface net downward shortwave and total radiative flux differences between the PP and CTL forecast runs are shown in Figure 6. The plots show significant decreases in shortwave fluxes over continents as well

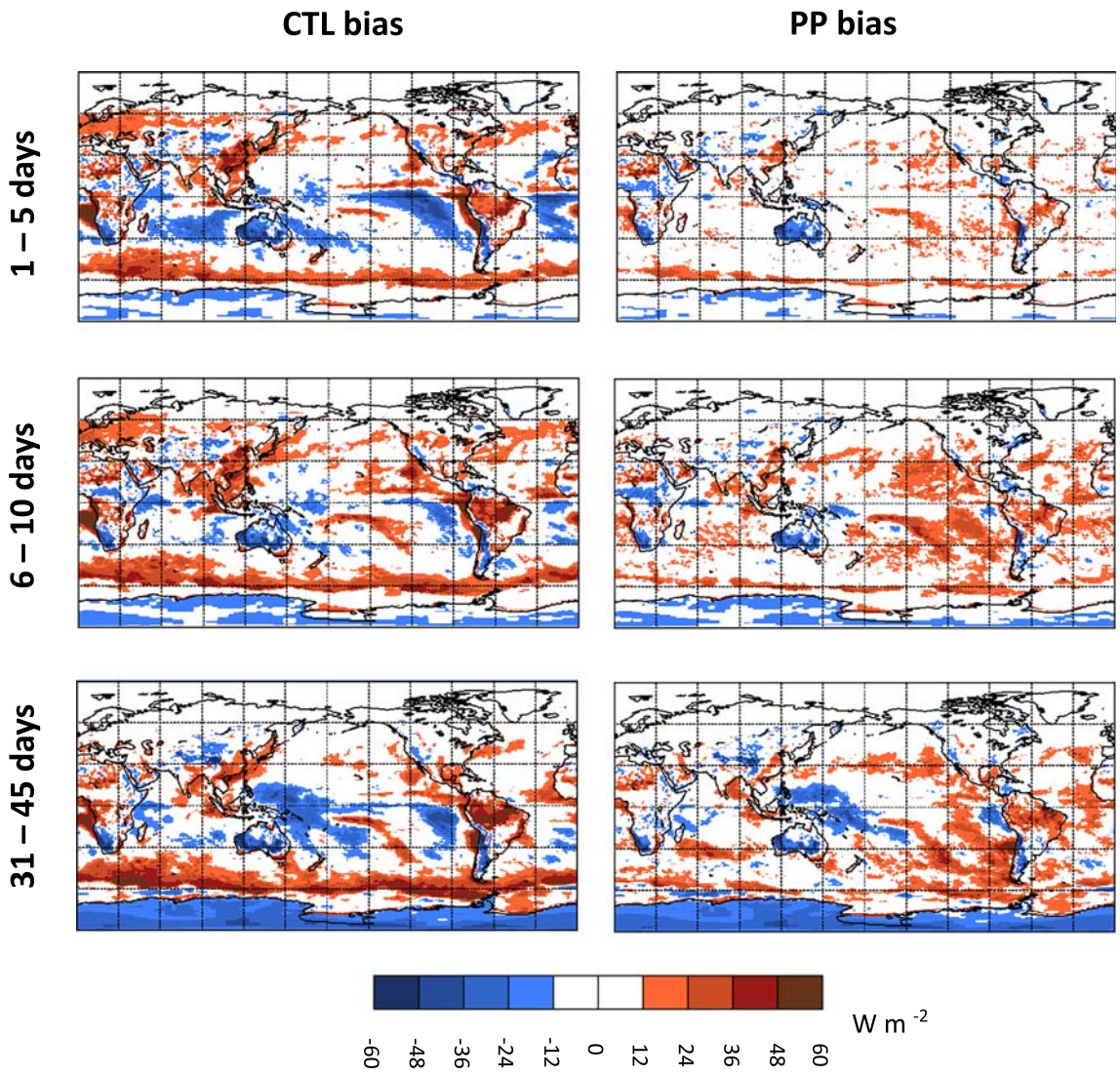

Figure 7. Surface net downward shortwave radiative flux bias (W m^{-2}) for the PP and CTL runs for different lead-time averaging intervals.

as high-latitude oceanic regions. Over many tropical and subtropical oceanic regions the shortwave and total radiative fluxes are increased. The associated changes in the flux biases compared to CERES data are shown in Figures 7 and 8, respectively. Clearly, there are some very significant improvements in the surface shortwave fluxes in the PP run during the first five days of the forecasts. The improvements over land tend to persist fairly well to longer lead times, as do some improvements in the far eastern tropical and subtropical Pacific and over the Southern Ocean. Over a number of oceanic regions, however, positive biases increase significantly by days 6–10. This occurs particularly over some of the subtropical low cloud regions. Errors in these regions are known to be sensitive to details of the atmospheric boundary layer physics, and it is unclear the extent to which feedbacks from changes in neighboring regions may also play a role. In addition, as noted above, due to lead-time dependent system biases the optimality of parameter perturbations computed based on forecast lead times in the range of 6–12 hours (as outlined in section 2) may be impaired at longer lead times. Overall, the shortwave results appear promising, with clear improvements early on, and overall positive results through all lead-time categories. The changes in the surface net downward total radiative flux biases (Figure 8) are somewhat more limited than for the shortwave fluxes, as differences in the longwave fluxes (inferred from comparison with Figure 7) tend to moderate the time-mean changes in the shortwave fluxes. The Tropics and the Southern Ocean

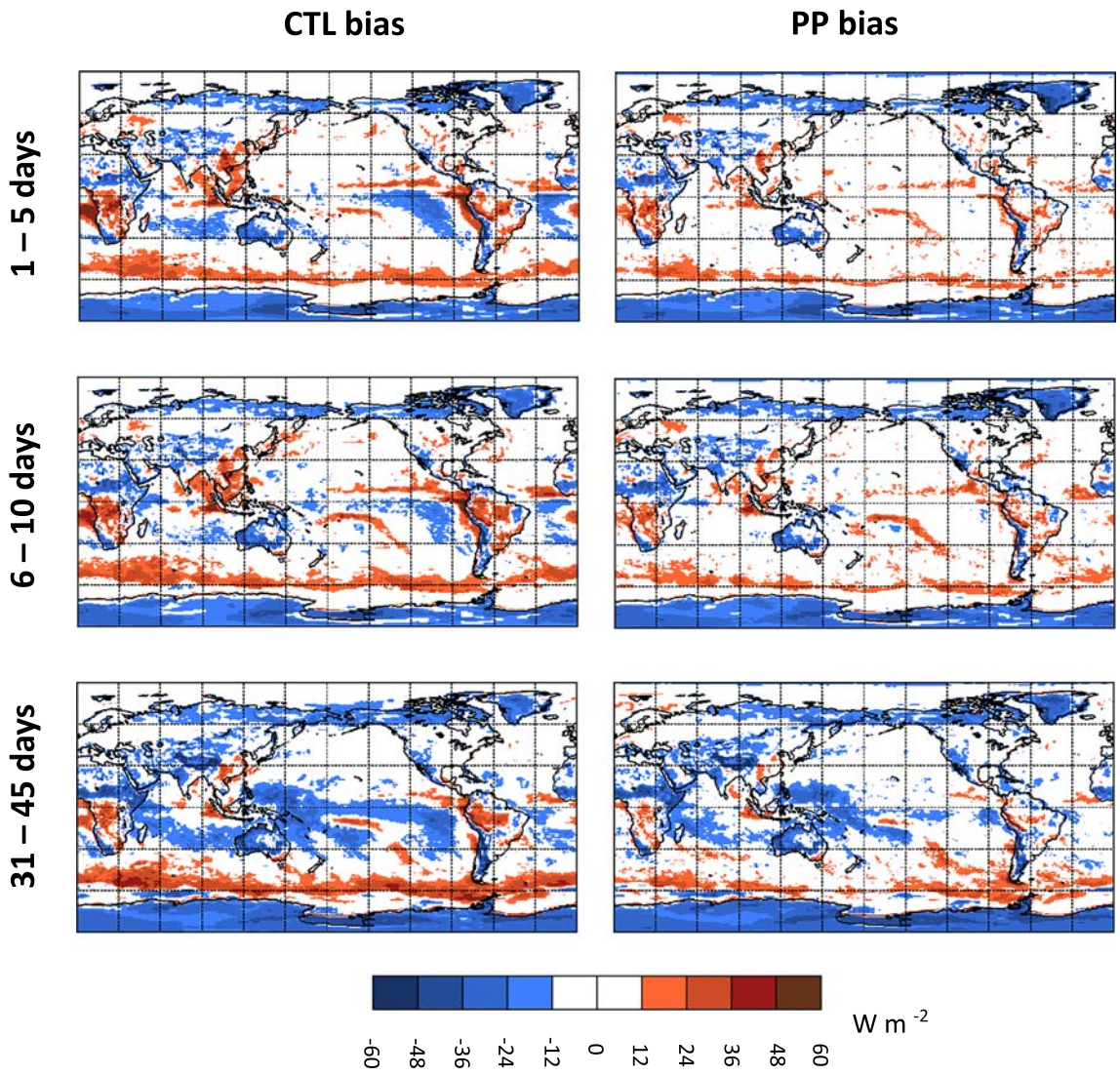

Figure 8. Surface net downward total radiative flux bias (W m^{-2}) for the PP and CTL runs for different lead-time averaging intervals.

nonetheless do show some significant improvements in the PP run, which in many areas persist through all lead-time categories.

A direct comparison of the degree to which the surface radiative fluxes are improved in the PP forecast runs is shown in Figure 9 in which the differences in absolute biases in the surface net downward shortwave and total radiative fluxes between the PP and CTL forecasts are plotted. Negative (blue) values represent improvement in these plots. The color scale in Figure 9 is half that in Figures 7 and 8 to better show the geographical extent of the changes in absolute bias. One finds that the PP run has clearly overall smaller biases than the CTL run for short lead times for both the shortwave and total radiative fluxes. As the runs progress the results are somewhat more mixed, with the growing positive biases in the surface downward shortwave flux over many noncoastal ocean regions (Figure 7) contributing to areas of net increase in absolute bias. Nonetheless, the global mean absolute bias decreases for all lead time intervals for both the shortwave and total radiative fluxes. The global mean error statistics are summarized in Tables 2 and 3 for the surface shortwave and total radiative flux errors, respectively. Table 2 shows that for lead times of 1–5 days the MAE (mean absolute error) of the surface net shortwave flux improves by 5.1 W m^{-2} in the global mean, a reduction of 40 percent. The improvement is 2.5 W m^{-2} for lead times in the 31–45 day interval, a reduction of 18 percent. The MAE of the surface net total radiative flux (Table 3) improves by 2.3 W m^{-2} in the global mean

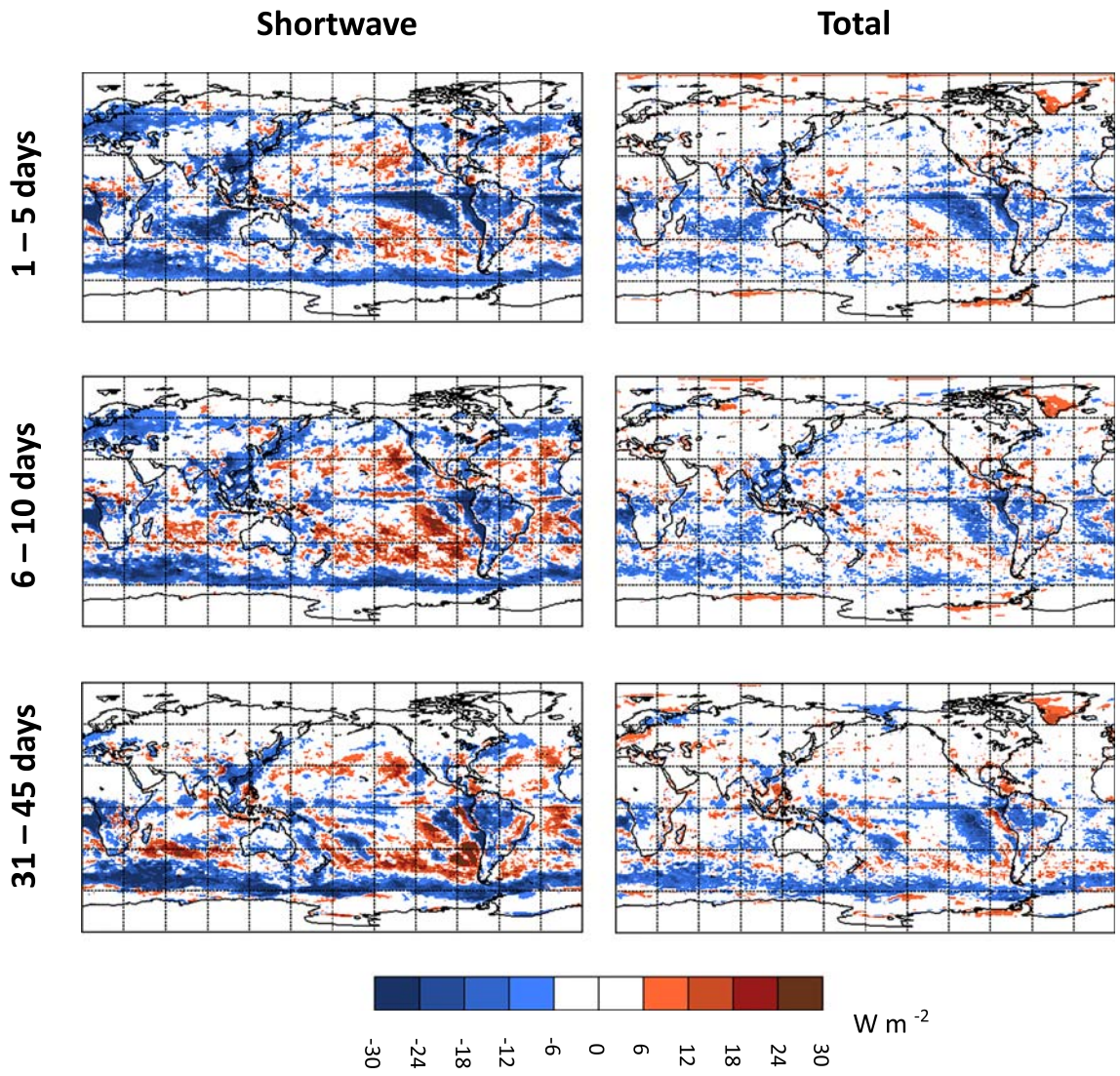

Figure 9. Difference in the absolute bias in surface net downward shortwave and total radiative fluxes between the PP and CTL runs (PP – CTL) for different lead-time averaging intervals. Negative (blue) values represent improvement in these plots.

for lead times of 1–5 days (reduction of 21 percent) and by 1.7 W m^{-2} for lead times of 31–45 days (reduction of 13 percent). As implied by these statistics, the improvements in surface net total radiative flux are due to the improved shortwave fluxes, and indeed the MAE of the net surface longwave flux is essentially unchanged (improved by less than 1 percent for all three lead-time categories). A corresponding analysis in terms of the global mean RMSE gives similar results, with an improvement of 37 percent in the surface net shortwave flux for lead times from 1–5 days, decreasing to 18 percent for lead times from 31–45 days. The global mean RMSE of the surface net longwave flux (not shown) is essentially unchanged (a slight degradation of 2 percent for lead times from 1–5 days, decreasing to a 0.5 percent increase for lead times of 31–45 days). The tables include the corresponding error reductions obtained when the only contributions included are those from grid points for which a Student's t-test ascribes a statistical significance of the mean bias difference between the PP and CTL runs at above the 95 percent

Table 2
Changes in global mean surface net shortwave flux errors (PP-CTL) (W m^{-2})

	ΔMAE		ΔRMSE	
Lead time	All	Stat. Sig.	All	Stat. Sig.
1–5 days	−5.1 (−40%)	−3.4	−6.3 (−37%)	−7.2
6–10 days	−2.8 (−21%)	−1.3	−3.8 (−22%)	−3.7
31–45 days	−2.5 (−18%)	−1.8	−3.3 (−18%)	−4.1

Note. "Stat. Sig." denotes results restricted to bias differences for which a Student's t-test assigns a significance at greater than the 95 percent level.

Table 3
Changes in global mean surface net radiative flux errors (PP-CTL) (W m^{-2})

	ΔMAE		ΔRMSE	
Lead time	All	Stat. Sig.	All	Stat. Sig.
1–5 days	−2.3 (−21%)	−1.1	−2.3 (−16%)	−3.1
6–10 days	−1.8 (−16%)	−0.6	−1.8 (−12%)	−2.1
31–45 days	−1.7 (−13%)	−1.1	−1.7 (−10%)	−2.5

Note. "Stat. Sig." denotes results restricted to bias differences for which a Student's t-test assigns a significance at greater than the 95 percent level.

level. Although the 15-forecast sample size is small, the statistically significant improvements obtained are generally a substantial fraction of the values obtained from the raw data, and in some cases larger.

In concluding our analysis of the initial trial tests of this parameter adjustment method, it is helpful to examine the impact on ground temperature/SST, which is directly affected by changes in the surface net radiative flux. Figure 10 shows the difference in the absolute value of the mean bias error in ground temperature/SST based on self-analysis at 12Z between the PP and CTL forecast runs for various lead-time categories. Note that for this comparison, 29 November 2013 was excluded as a verification date due to lost/damaged data. Results are shown separately for the entire globe and just for the non-polar oceans/lakes to adjust the shading scale for the differences in magnitude of the response. Globally, the mean of the bias error magnitude differences in Figure 10 (the MAE) for each lead-time category reflects an improvement in the PP runs. The global mean improvements decrease on a percentage basis

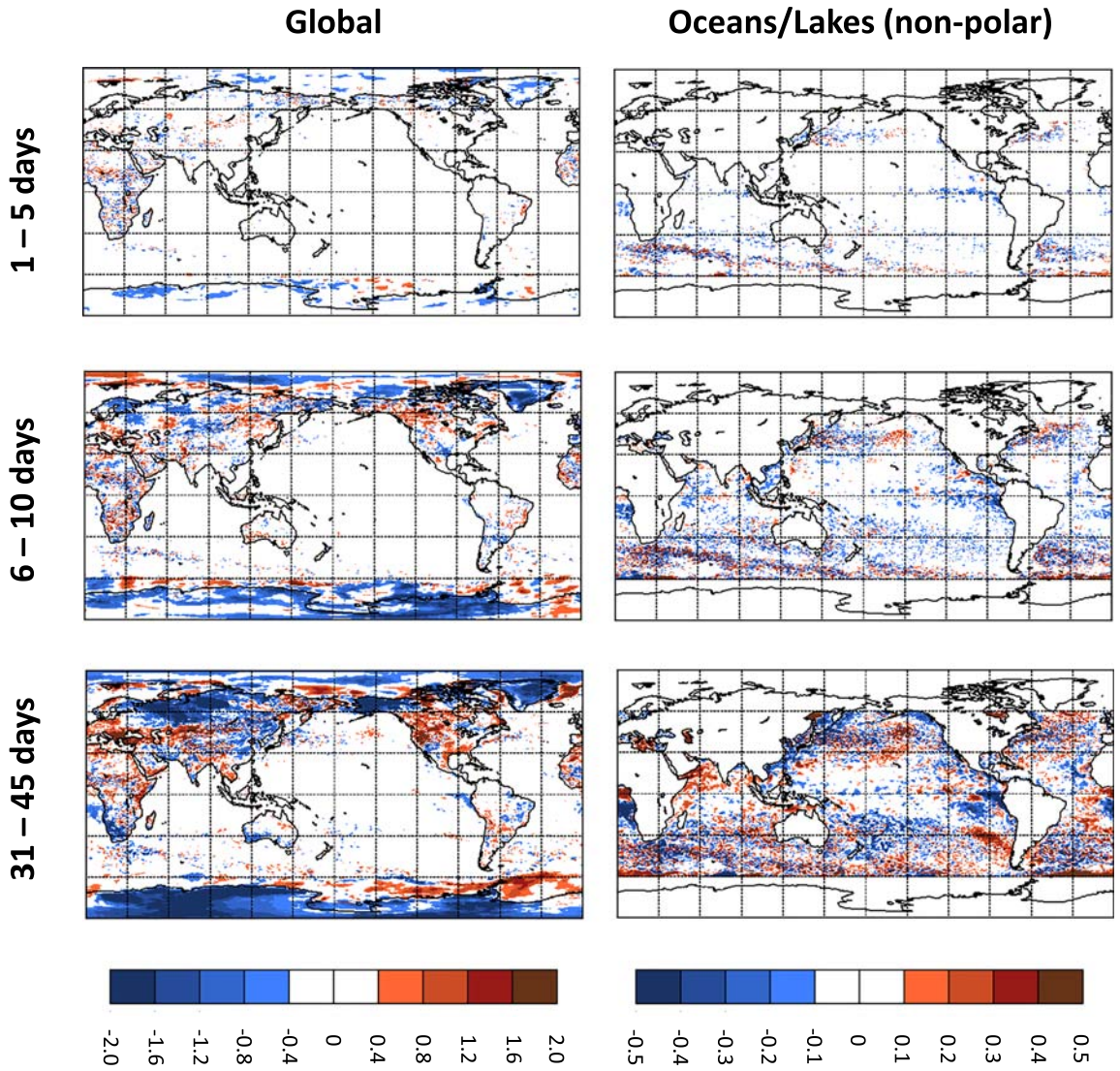

Figure 10. Difference in the absolute bias in ground temperature/SST (deg K) computed based on self-analysis for the PP and CTL runs (PP – CTL). Results are shown both globally and just over non-polar (60°N - 60°S) oceans/lakes to account for differences in scale. Negative (blue) values represent improvement in these plots.

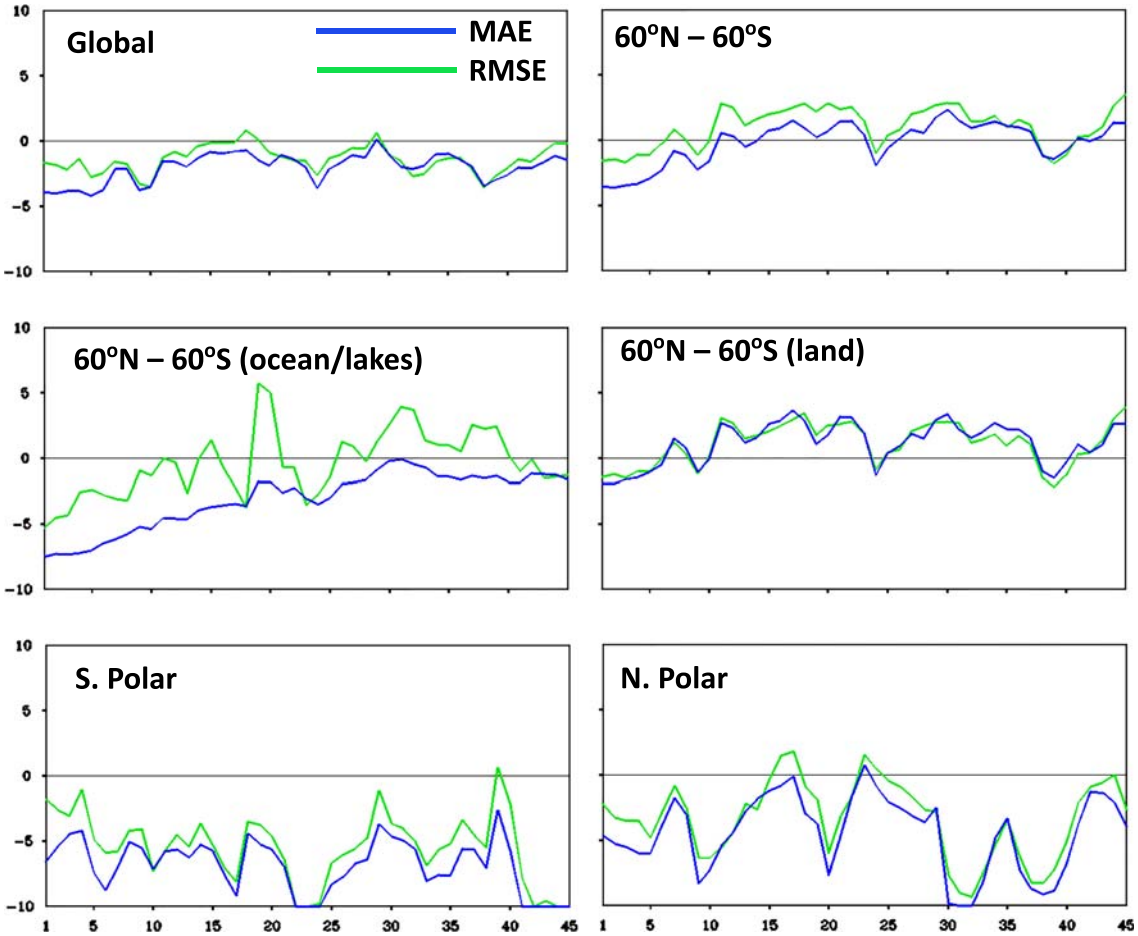

Figure 11. The curves show the percentage change in the self-analysis ground temperature/SST errors as a function of lead time (days) for various regions. The blue curves show the results for MAE, and the green curves the results for RMSE. The boundaries of the southern and northern polar regions are defined here by the respective 60^{o} latitude lines.

as the runs progress, ranging from 4.0 percent for days 1–5 to 3.1 percent for days 6–10 and 2.0 percent for days 31–45. Over the non-polar oceans/lakes, the mean improvements range from 7.2 percent for days 1–5, decreasing to 5.8 percent for days 6–10 and 1.3 percent for days 31–45. Figure 11 shows the percentage

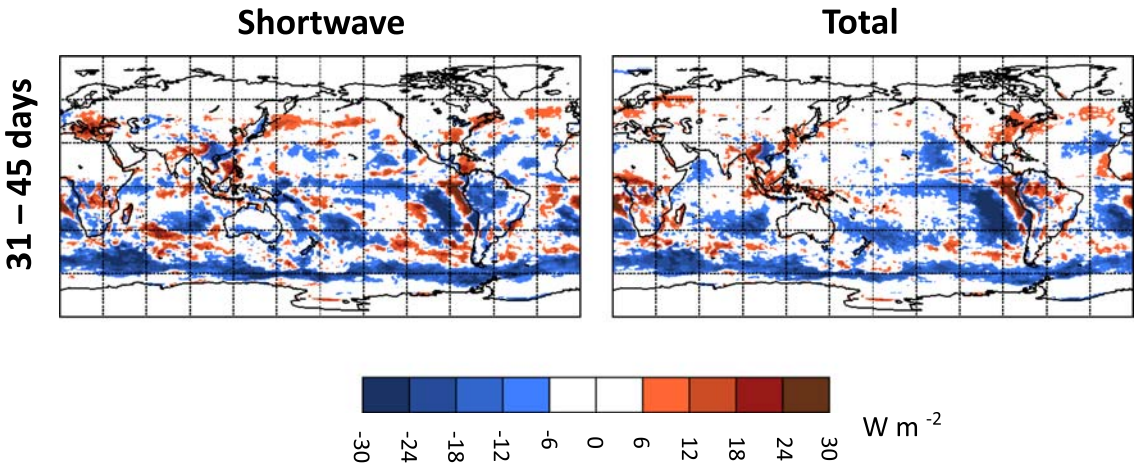

Figure 12. Difference in the absolute bias in TOA net downward shortwave and total radiative fluxes between the PP and CTL runs (PP – CTL) for 31–45 day lead times. Negative (blue) values represent improvement in these plots.

change in the self-analysis error as a function of lead time for various regions. Results for both MAE and RMSE show improvements globally. The global improvement though significant is found to be limited by the changes over land, for which errors are increased after approximately day 5. It is possible that inclusion of longwave fluxes in the adjustment procedure would help to reduce or eliminate this unwanted result. Also, it is not clear to what extent the details of the treatment of the land surface in the model may contribute to the current findings (e.g., Kowalczyk et al., 2016).

4. Summary and Discussion

A simple procedure for gradually but systematically adjusting a key parameter in the stratiform cloud cover parameterization in the Navy ESPC system to reduce biases in the surface net downward shortwave radiative flux is presented. As described in section 2, regionally varying adjustments to the k_3 parameter in the Xu-Randall cloud fraction scheme are made once per day based on shortwave radiative flux sensitivities to cloud cover perturbations computed during the short forecasts of the DA cycle. In this initial implementation of the scheme, daily mean surface net shortwave fluxes from the NASA CERES dataset are used to guide the parameter adjustments. Corresponding daily-mean shortwave fluxes are constructed from fluxes computed for lead times between 6–12 h in the 6-hourly DA cycle forecasts. Local comparisons of flux biases for small perturbations to the k_3 parameter determine whether the parameter is adjusted at a given location for a given day of the DA cycle. In this procedure, only small (factor of 0.02) fractional changes to the parameter are allowed at a given time in an effort to avoid generation of overly noisy distributions of the parameter perturbation. Though the daily changes are small, this nudging approach results in the development of significant regional variations in the k_3 parameter over the course of one to two weeks.

In section 3 results from initial testing of the parameter adjustment procedure in the Navy ESPC system are presented. Two sets of runs were carried out, a Control (CTL) run and a "Perturbed Parameter" (PP) run (see Table 1). The system was given a 31-day spin-up period beginning July 31, 2013. Reductions in the surface radiative flux biases at the short lead times (6–12 h) for which the parameter perturbations are computed are found to be substantial, as shown in Figure 3. In a series of 15 45-day forecasts initiated at 5-day intervals in the period following the initial spin-up (beginning at 12Z on 1 Sept., 2013), positive impacts of the parameter perturbations computed during the DA cycle are documented for several lead-time categories. Improvements in surface shortwave radiative fluxes are most notable in the 1–5 day range (Figure 7), but significant benefits of the approach persist into the post 30-day period. After five days, improvements are partially offset by the development of enhanced positive biases over some subtropical oceanic regions. In contrast somewhat to the impact on shortwave flux biases, improvements to the corresponding total downward radiative flux biases are more modest (Figure 8), but are more uniformly positive through the duration of the forecasts. As summarized in Tables 2 and 3 the adjustment procedure reduces the global mean MAE and RMSE of the surface net shortwave and total radiative flux biases for both short and longer range lead-time categories.

Although not the focus in this study, radiative flux results for the top of the atmosphere (TOA) appear to be encouraging as well. Unfortunately, the saved TOA shortwave flux data are limited to instantaneous values available once every three hours (rather than time-averages over all time steps as is the case with the surface data); hence the diurnal cycle is not resolved to the extent one would desire. With this limitation in mind, the changes in absolute bias of the TOA shortwave and net radiative fluxes for lead times from 31–45 days are plotted in Figure 12. The results clearly show improvements similar in many respects to the corresponding results for the surface in the two lower panels of Figure 9.

Impacts of the parameter perturbations on ground and sea surface temperature errors are illustrated in Figures 10 and 11. Globally, the associated MAE and RMSE based on self-analysis are improved on average through most of the duration of the 45-day forecasts. Impacts over the oceans and polar regions are generally positive, with some degradation over non-polar land areas. The significant improvements in the temperature errors over Antarctica are notable in that the differences there in the surface radiative fluxes are quite small (Figure 6.). It seems that the significant improvements achieved in the radiative flux biases in the Southern Ocean (Figures 7 and 8) may be having a beneficial non-local impact in this regard. The parameter adjustment in this area reduces what on average is a positive surface net shortwave flux bias, a common problem

in coupled models which has been attributed to difficulties in representing the effects of supercooled liquid clouds in the region (e.g. Bodas-Salcedo et al., 2016).

The work reported here is notably part of a broader ongoing effort at the Naval Research Laboratory to reduce surface flux biases in Navy forecast systems. Development of the Navy ESPC system has benefited from the substantial experience at NRL with HYCOM in the (uncoupled) GOFS system. Currently in GOFS a surface net heat flux bias correction is applied for short lead-time forecasts (out to 7 days) based on sea surface temperature errors from a one-year series of forecasts. An updated approach is under development to correct the flux biases at the air-sea interface based on in situ and remote sensing observations of the radiative fluxes and inputs to turbulent flux parameterizations. The results from the present study suggest that a parameter adjustment procedure within the atmospheric model component of the system may be a workable alternative/adjunct to these approaches in the case of radiative flux biases. The current method in principle allows for an automated response of the model tuning to a range of factors, including for example, changes in model resolution or physics components, as well as seasonal and climate changes. In addition, optimization solely within the context of the full resolution forecast system precludes any possibility of unwanted effects stemming from physics tuning within a lower-resolution ensemble configuration. Although the development and testing of the scheme has thus far utilized the CERES dataset, which has a latency of about six months before becoming available, utilization of the CERES FLASHFlux product (Kratz et al., 2014), which is available on a near real-time basis (about one week), may provide a route to operational applicability.

Further improvements in the current implementation can be envisioned, including the utilization of longwave radiative flux data in addition to the shortwave flux data used here to adjust the *k3* parameter. Also, the focus here on a single parameter has its limitations, and ideally one should consider how the change in one parameter may impact the optimal value of other parameters (e.g., McLay & Liu, 2014; Posselt & Vukicevic, 2010). It should be noted that extension of the method to more than one parameter, or a multi-valued parameter, could be possible without excessive cost. However, since the method relies on the ability to determine the sensitivity of observable quantities such as fluxes to parameter perturbations without actually computing modified forecast trajectories, the extensibility of the scheme is in some ways limited. An enhanced implementation of the scheme that includes correlated adjustments to the effective size of cloud droplets and/or ice crystals in the radiation code is being considered as a means to help improve the overall impact on surface radiative fluxes. Finally, it is significant that in these forecasts the k_3 parameter perturbations are kept fixed at their values on the date of the forecast initiation. Other treatments, such as adjustment at long lead times to climatological values, or even zero, suggest themselves as well for future testing.

Appendix A.

The parameterization of convective cloud cover in NAVGEM is an extension of the treatment of Slingo (1987). The NAVGEM treatment replaces the vertical profile of cloudiness assumed in the Slingo scheme with a relative humidity *RH* dependent scaling given by

$$cf_{conv} = cf_{conv\_cb} f(RH, \rho)/f(RH_{cb}, \rho_{cb}), \tag{A1}$$

where cf_{conv} is convective cloud fraction, ρ is density, and the subscript *cb* designates cloud base values. The convective cloud cover at cloud base cf_{conv_cb} is assumed to vary with convective rainfall rate *rain* (cm h^{-1}) as in Slingo (1987), but with a scaling by cloud base mass flux mf_{cb}:

$$cf_{conv\_cb} = 1.2\left(\frac{0.93 + 0.124\ln(rain + 0.001)}{0.93 + 0.124\ln(0.001)}\right) mf_{cb}, \tag{A2}$$

The mass flux scaling allows the convective cloud fraction to smoothly approach zero in the limit as parameterized nonprecipitating convective activity vanishes. Cloud cover variations above cloud base are parameterized by the function *f (RH,ρ)* given by

$$f(RH,\rho) = \frac{6\exp[-2[1-RH]]\rho_{cb}}{[1+10[1-RH]]\rho}, \tag{A3}$$

which was formulated to roughly represent various impacts of moisture on cloud cover, as well as parcel expansion upon lifting through cloud base to various detrainment levels.

In addition to its use as an input to the RRTMG radiation scheme for computing radiative fluxes, the convective cloud cover in NAVGEM is also used to estimate the portion of the prognostic cloud liquid and ice condensate q_t associated with stratiform cloud cover for use in the Xu-Randall cloud fraction scheme. The moist mixing ratio of the stratiform condensate q_c is thus obtained simply as

$$q_c = \max(q_t - cf_{conv}\ q_{conv}, 0.), \tag{A4}$$

where q_{conv} is a crude estimate (cf. Ridout et al., 1994) of the condensate mixing ratio within the convective cloud-covered region. Although in many cases the prognostic cloud condensate is in fact identically equal to the stratiform condensate, as described in Hogan et al. (2014) the extension of the cloud scheme of Zhao and Carr 1997 in NAVGEM provides for enhanced retention on the grid-scale of condensate detrained from convective clouds in the presence of ongoing convection. This feature was deemed necessary in order to help ensure a sufficient radiative 'footprint' of convective clouds based on comparisons with TRMM cloud liquid water retrievals.

Acknowledgments
This research was sponsored by OPNAV N2N6E and the Office of Naval Research's Earth System Prediction Capability, PE0603207N. The work was supported in part by a grant of computing time from the Department of Defense's (DoD's) High Performance Computing Modernization Program (HPCMP). The helpful comments of two anonymous reviewers are gratefully acknowledged. The CERES data are provided by the NASA Langley Research Center Atmospheric Science Data Center (https://eosweb.larc.nasa.gov/order-data). The Navy ESPC analysis and forecast data are stored at the Navy DoD Supercomputing Resource Center (DSRC). Access to the Navy DSRC may be obtained through a request to the DoD HPCMP (https://www.hpc.mil/). Once an account has been established, the corresponding author may be contacted for information to access the archived data.

References

Aksoy, A., Zhang, F., & Nielsen-Gammon, J. W. (2006). Ensemble-based simultaneous state and parameter estimation with MM5. *Geophysical Research Letters*, *33*, L12801. https://doi.org/10.1029/2006GL026186

Anderson, J. L. (2001). An ensemble adjustment Kalman filter for data assimilation. *Monthly Weather Review*, *129*, 2884–2903. https://doi.org/10.1175/1520-0493(2001)129<2884:AEAKFF>2.0.CO;2

Bleck, R. (2002). An oceanic general circulation model framed in hybrid isopycnic-Cartesian coordinates. *Ocean Modelling*, *4*, 55–88. https://doi.org/10.1016/S1463-5003(01)00012-9

Bodas-Salcedo, A., Hill, P. G., Furtado, K., Williams, K. D., Field, P. R., Manners, J. C., et al. (2016). Large contribution of supercooled liquid clouds to the solar radiation budget of the Southern Ocean. *Journal of Climate*, *29*, 4213–4228. https://doi.org/10.1175/JCLI-D-15-0564.1

Calisto, M., Folini, D., Wild, M., & Bengtsson, L. (2014). Cloud radiative forcing intercomparison between fully coupled CMIP5 models and CERES satellite data. *Annales Geophysicae*, *32*, 793–807. https://doi.org/10.5194/angeo-32-793-2014

Cess, R. D., Potter, G. L., Blanchet, J. P., Boer, G. J., del Genio, A. D., Déqué, M., et al. (1990). Intercomparison and interpretation of climate feedback processes in 19 atmospheric general circulation models. *Journal of Geophysical Research*, *95*(D10), 16601–16,615. https://doi.org/10.1029/JD095iD10p16601

Doelling, D. R., Loeb, N. G., Keyes, D. F., Nordeen, M. L., Morstad, D., Nguyen, C., et al. (2013). Geostationary enhanced temporal interpolation for CERES flux products. *Journal of Atmospheric and Oceanic Technology*, *30*, 1072–1090. https://doi.org/10.1175/JTECH-D-12-00136.1

Hacker, J. P., & Snyder, C. (2005). Ensemble Kalman filter assimilation of fixed screen-height observations in a parameterized PBL. *Monthly Weather Review*, *133*, 3260–3275. https://doi.org/10.1175/MWR3022.1

Hansen, J., & Penland, C. (2007). On stochastic parameter estimation using data assimilation. *Physica D*, *230*, 88–98. https://doi.org/10.1016/j.physd.2006.11.006

Harshvardhan, R., Davies, D., Randall, A., & Corsetti, T. G. (1987). A fast radiation parameterization for atmospheric circulation models. *Journal of Geophysical Research*, *92*(D1), 1009–1016. https://doi.org/10.1029/JD092iD01p01009

Hogan, T. F., Liu, M., Ridout, J., Peng, M., Whitcomb, T., Ruston, B., et al. (2014). The Navy global environmental model. *Oceanography*, *27*(3), 116–125. https://doi.org/10.5670/oceanog.2014.73

Hogan, T. F., & Rosmond, T. E. (1991). The description of the Navy operational global atmospheric prediction System's spectral forecast model. *Monthly Weather Review*, *119*, 1786–1815. https://doi.org/10.1175/1520-0493(1991)119%3C1786:TDOTNO%3E2.0.CO;2

Hourdin, F., Mauritsen, T., Gettelman, A., Golaz, J. C., Balaji, V., Duan, Q., et al. (2017). The art and science of climate model tuning. *Bulletin of the American Meteorological Society*, *98*(3), 589–602. https://doi.org/10.1175/BAMS-D-15-00135.1

Hunke, E. C., & Lipscomb, W. H. (2010). CICE: The Los Alamos Sea Ice Model documentation and software user's manual version 4.1. Los Alamos National Laboratory T-3 Fluid Dynamics Group Tech. Rep. LA-CC-06-012, 76 pp.

Iacono, M. J., Delamere, J. S., Mlawer, E. J., Shephard, M. W., Clough, S. A., & Collins, W. D. (2008). Radiative forcing by longlived greenhouse gases: Calculations with the AER radiative transfer models. *Journal of Geophysical Research*, *113*, D13103. https://doi.org/10.1029/2008JD009944

Janiga, M. A., Schreck, C., Ridout, J. A., Flatau, M., Barton, N., Metzger, E. J., & Reynolds, C. (2018). Subseasonal forecasts of convectively coupled equatorial waves and the MJO: Activity and predictive skill. *Monthly Weather Review*, *146*, 2337–2360. https://doi.org/10.1175/MWR-D-17-0261.1

Kowalczyk, L., Stevens, E., Law, R. M., Harman, I. N., Dix, M., Franklin, C. N., & Wang, Y.-P. (2016). The impact of changing the land surface scheme in ACCESS(v1.0/1.1) on the surface climatology. *Geoscientific Model Development*, *9*, 2771–2791. https://doi.org/10.5194/gmd-9-2771-2016

Kratz, D. P., Stackhouse, P. W. Jr., Gupta, S. K., Wilber, A. C., Sawaengphokhai, P., & McGarragh, G. R. (2014). The fast Longwave and shortwave flux (FLASHFlux) data product: Single-scanner footprint fluxes. *Journal of Applied Meteorology and Climatology*, *53*, 1059–1079. https://doi.org/10.1175/JAMC-D-13-061.1

Li, S., Zhang, S., Liu, Z., Lu, L., Zhu, J., Zhang, X., et al. (2018). Estimating convective parameters in the GFDL CM2.1 model using ensemble data assimilation. *Journal of Advances in Modelling Earth Systems*, *10*, 989–1010. https://doi.org/10.1002/2017MS001222

Liu, Y., Liu, Z., Zhang, S., Rong, X., Jacob, R., Wu, S., & Lu, F. (2014). Ensemble based parameter estimation in a coupled GCM using the adaptive spatial average method. *Journal of Climate*, *27*, 4002–4014. https://doi.org/10.1175/JCLI-D-13-00091.1

McLay, J. G., & Liu, M. (2014). Detecting dependence in the sensitive parameter space of a model using statistical inference and large forecast ensembles. *Monthly Weather Review*, *142*(10), 3734–3755. https://doi.org/10.1175/MWR-D-13-00340.1

Metzger, E. J., Smedstad, O. M., Thoppil, P., Hurlburt, H., Cummings, J., Walcraft, A., et al. (2014). US Navy operational global ocean and arctic ice prediction systems. *Oceanography*, *27*(3), 32–43. https://doi.org/10.5670/oceanog.2014.66

Ollinaho, P., Lock, S.-J., Leutbecher, M., Bechtold, P., Beljaars, A., Bozzo, A., et al. (2017). Towards process-level representation of model uncertainties: Stochastically perturbed parametrizations in the ECMWF ensemble. *Quarterly Journal of the Royal Meteorological Society*, *143*, 408–422. https://doi.org/10.1002/qj.2931

Posselt, D. J., & Bishop, C. H. (2012). Nonlinear parameter estimation: Comparison of an ensemble Kalman smoother with a Markov chain Monte Carlo algorithm. *Monthly Weather Review*, *140*, 1957–1974. https://doi.org/10.1175/MWR-D-11-00242.1

Posselt, D. J., & Vukicevic, T. (2010). Robust characterization of model physics uncertainty for simulations of deep moist convection. *Monthly Weather Review*, *138*, 1513–1535. https://doi.org/10.1175/2009MWR3094.1

Reynolds, C. A., Ridout, J. A., & Mclay, J. G. (2011). Examination of parameter variations in the U. S. Navy Global Ensemble. *Tellus A*, *63*(5), 841–857. https://doi.org/10.1111/j.1600-0870.2011.00532.x

Ridout, J. A., Chertock, B., & Gelaro, R. (1994). Response of a general circulation model to a change in cloud solar forcing: Model feedbacks and comparison with satellite data. *Journal of Geophysical Research*, *99*(D9), 18,555–18,576. https://doi.org/10.1029/94JD00359

Schmidt, G. A., Bader, D., Donner, L. J., Elsaesser, G. S., Golaz, J.-C., Hannay, C., et al. (2017). Practice and philosophy of climate model tuning across six US modeling centers. *Geoscientific Model Development*, *10*(9), 3207–3223. https://doi.org/10.5194/gmd-10-3207-2017

Slingo, J. M. (1987). The development and verification of a cloud prediction scheme for the ECMWF model. *Quarterly Journal of the Royal Meteorological Society*, *113*, 899–927. https://doi.org/10.1002/qj.49711347710

Sumata, H., Kauker, F., Gerdes, R., Köberle, C., & Karcher, M. (2013). A comparison between gradient descent and stochastic approaches for parameter optimization of a sea ice model. *Ocean Science*, *9*, 609–630. https://doi.org/10.5194/os-9-609-2013

Wu, X., Zhang, S., Liu, Z., Rosati, A., Delworth, T., & Liu, Y. (2012). Impact of geographic dependent parameter optimization on climate estimation and prediction: Simulation with an intermediate coupled model. *Monthly Weather Review*, *140*, 3956–3971. https://doi.org/10.1175/MWR-D-11-00298.1

Xu, K.-M., & Randall, D. A. (1996a). A semiempirical cloudiness parameterization for use in climate models. *Journal of the Atmospheric Sciences*, *53*, 3084–3102. https://doi.org/10.1175/1520-0469(1996)053%3C3084:ASCPFU%3E2.0.CO;2

Xu, K.-M., & Randall, D. A. (1996b). Explicit simulation of cumulus ensembles with the GATE phase III data: Comparison with observations. *Journal of the Atmospheric Sciences*, *53*, 3710–3736. https://doi.org/10.1175/1520-0469(1996)053%3C3710:ESOCEW%3E2.0.CO;2

Ye, Q.-Z., & Chen, S.-S. (2013). The ultimate meteorological question from observational astronomers: How good is the cloud cover forecast? *Monthly Notices of the Royal Astronomical Society*, *428*, 3288–3294. https://doi.org/10.1093/mnras/sts278

Yin, J., & Porporato, A. (2017). Diurnal cloud cycle biases in climate models. *Nature Communications*, *8*(1), 2269. https://doi.org/10.1038/s41467-017-02369-4

Zebiak, S. E., & Cane, M. A. (1987). A model El Nino–southern oscillation. *Monthly Weather Review*, *115*, 2262–2278. https://doi.org/10.1175/1520-0493(1987)115,2262:AMENO.2.0.CO;2

Zhao, Q., & Carr, F. H. (1997). A Prognostic Cloud Scheme for Operational NWP Models. *Monthly Weather Review*, *125*(8), 1931–1953. https://doi.org/10.1175/1520-0493(1997)1252.0.co;2

Zhao, Y., Liu, Z., Zheng, F., & Jin, Y. (2019). Parameter optimization for real-world ENSO forecast in an intermediate coupled model. *Monthly Weather Review*, *147*, 1429–1445. https://doi.org/10.1175/MWR-D-18-0199.1